Correlation between glass transition temperature and molecular mass in non-polymeric and polymer glass formers

ARTICLE *in* POLYMER · DECEMBER 2013

Impact Factor: 3.56 · DOI: 10.1016/j.polymer.2013.11.002

2 AUTHORS:

Vladimir N Novikov
Oak Ridge National Laboratory
150 PUBLICATIONS **3,477** CITATIONS
SEE PROFILE

Ernst Rössler
University of Bayreuth
205 PUBLICATIONS **5,485** CITATIONS
SEE PROFILE

THE JOURNAL OF PHYSICAL CHEMISTRY B

Article

pubs.acs.org/JPCB

Interplay Between Hydrophobic Aggregation and Charge Transport in the Ionic Liquid Methyltrioctylammonium Bis(trifluoromethylsulfonyl)imide

Philip J. Griffin,[†] Adam P. Holt,[†] Yangyang Wang,[∥] Vladimir N. Novikov,[‡] Joshua R. Sangoro,*[,§] Friedrich Kremer,[⊥] and Alexei P. Sokolov*[,†,∥,‡]

[†]Department of Physics and Astronomy, [‡]Department of Chemistry, and [§]Department of Chemical and Biomolecular Engineering, University of Tennessee, Knoxville, Tennessee 37996-1600, United States

[∥]Chemical Sciences Division, Oak Ridge National Laboratory, Oak Ridge, Tennessee 37830-6197, United States

[⊥]Institute of Experimental Physics, University of Leipzig, Linnestr. 5, 04103 Leipzig, Germany

ABSTRACT: In order to understand the nature of the exceedingly low ionic conductivity of aprotic ammonium ionic liquids (ILs), we have measured the charge transport and structural dynamics of methyltrioctylammonium bis-(trifluoromethylsulfonyl)imide [m3oa][ntf2] over a broad temperature range using broadband dielectric spectroscopy, depolarized dynamic light scattering (DDLS), rheology, and pulsed field gradient nuclear magnetic resonance. We demonstrate that the low level of ionic conductivity in this material is due to the combined effects of reduced ion mobility as well as reduced free ion concentration relative to other types of ILs. Furthermore, detailed analysis of the DDLS spectra reveals a slow process in addition to the structural α relaxation that we attribute to reorientational motion of alkyl aggregates. These findings indicate that hydrophobic aggregation strongly influences the charge transport mechanism of aprotic ammonium ionic liquids with long aliphatic side chains.

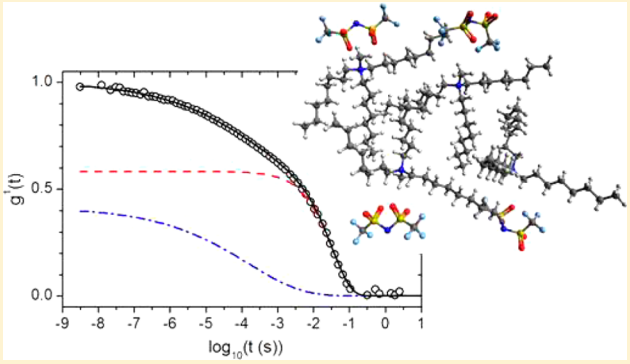

INTRODUCTION

Aprotic quaternary ammonium ionic liquids (ILs) are an important class of materials due to their high electrochemical stability and hydrophobicity.[1,2] However, many of these liquids have high viscosities and low ionic conductivities relative to other types of ILs—properties which prevent them from being utilized in electrochemical applications.[3] One of the main questions regarding ammonium ILs (and ILs in general) is how does the chemical structure of the constituent ions affect the morphology, dynamics, and charge transport mechanism in the liquid and supercooled liquid state. Furthermore, it is essential to understand how these properties are interconnected.

Recent experimental and simulation studies have indicated that complex mesoscopic morphologies may exist in the liquid state of many types of ILs.[4−7] Numerous ILs display a prepeak[8] in the static structure factor at low wave-vectors which some authors have interpreted as evidence for the existence of mesoscale organization.[9] Triolo et al. interpreted this peak in a series of imidazolium based ILs as arising from the aggregation of alkyl side chains, finding that the length scale associated with this prepeak was correlated with the length of the alkyl side chain.[10,11] Similar static structure prepeaks have also been observed in polyethylene side chain polymers, where correlations between prepeak position and alkyl chain length were attributed to hydrophobic aggregation.[12,13] Other authors have suggested that such prepeaks primarily arise from anion−anion correlations.[14−16] However, these authors have also acknowledged that the anion configurations may reflect the underlying presence of aggregated alkyl chains. Previous simulation studies of a set of short chained ILs have also suggested that the alkyl side chains aggregate into mesoscopic domains which are stable at low enough temperature and can execute collective diffusive motions.[17]

In contrast to the controversial topic of mesoscopic structures in short chained imidazolium based ILs, there is relatively wide agreement that hydrophobically aggregated alkyl tails are present in quaternary ammonium and phosphonium based ILs with side chains longer than butyl.[18−21] Recent simulation studies of a set of methyltrialkylammonium bis(trifluoromethylsulfonyl)imide [m3xa][ntf2] ILs demonstrated that as the length of the alkyl tails increases beyond butyl, the tails begin to aggregate into clusters which percolate the liquid medium and dominate the structural motif.[22] One of the important questions to ask regarding this phenomenon is how does the presence of hydrophobic aggregation affect the structural dynamics and charge transport properties in these types of ILs. While these properties have been well

Received: December 17, 2013
Published: January 3, 2014

   dx.doi.org/10.1021/jp412365n | J. Phys. Chem. B 2014, 118, 783−790

characterized over broad experimental conditions for many other types of ILs such as the imidazolium based liquids discussed above,[23−25] the transport properties of quaternary ammonium ILs have been studied in a much more limited capacity.

In this article we present measurements of the charge transport and structural dynamics in the quaternary ammonium IL methyltrioctylammonium bis(trifluoromethylsulfonyl)imide [m3oa][ntf2] from above the melting point down to the calorimetric glass transition measured via broadband dielectric spectroscopy (BDS), pulsed field gradient nuclear magnetic resonance (PFG NMR), depolarized dynamic light scattering (DDLS), and rheology. We have found that relative to other types of ILs with similar glass transition temperatures, the ionic conductivity of [m3oa][ntf2] is unusually low due to reduced ion mobility as well as a reduced concentration of free ions. Furthermore, a slow relaxation process is present in the DDLS spectra in addition to the structural α relaxation process which we attribute to the reorientational motions of aggregated alkyl nanodomains. Together, these findings indicate that the presence of hydrophobic aggregates significantly reduces ion mobility and also enhances counterion association in ILs with large concentrations of aliphatic moieties.

EXPERIMENTAL SECTION

The [m3oa][ntf2] sample was purchased from Iolitec USA (M_W = 648.85 g/mol, 99% purity). The chemical structure is depicted in Figure 1. Prior to measurements, the sample was

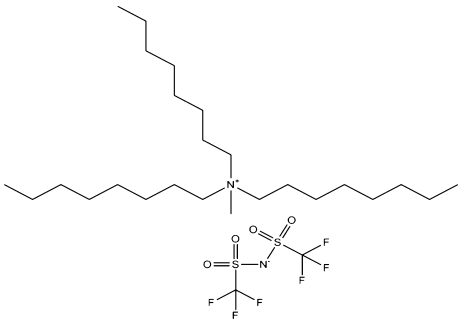

Figure 1. Chemical structure of methyltrioctylammonium bis(trifluoromethylsulfonyl)imide [m3oa][ntf2].

dried in a vacuum oven (P = 1 mbar) at 50 °C for 24 h to remove any residual water or dissolved gases. Following vacuum drying, the sample was filtered through 0.22 μm Teflon filters into cleaned, dried glass vials and quickly sealed under ambient conditions. The calorimetric glass transition temperature was determined to be T_g = 186 ± 2 K on cooling at 5 K/min using a Q1000 differential scanning calorimeter (TA Instruments). This value of T_g agrees well with recently reported DSC measurements of [m3oa][ntf2].[26]

Broadband dielectric spectroscopy (BDS) was used to characterize the charge transport and dipolar relaxations of [m3oa][ntf2] over a wide temperature range from 400 K down to 180 K. These measurements were performed using a Novocontrol Alpha-A dielectric analyzer in the frequency window 10^{-2} Hz to 10 MHz. The liquid sample was mounted between parallel 15 mm diameter stainless steel plates with small Teflon spacer posts used to maintain a plate distance of 0.1 mm. The temperature of the sample was controlled using a Novocontrol Quattro temperature control unit with stability of ±0.1 K.

Pulsed field gradient nuclear magnetic resonance (PFG NMR) measurements were performed using a 400 MHz NMR spectrometer with a home-built gradient device to obtain the self-diffusivities at selected temperatures. Additional details regarding the setup and measurement procedure can be found elsewhere.[23,27] A stimulated spin echo pulse sequence with observation time of 100 ms was used. The spin echo attenuation was monoexponential in the entire temperature range probed.

Depolarized dynamic light scattering (DDLS) measurements were performed to characterize the structural dynamics of [m3oa][ntf2] in a broad temperature (250 K down to T_g) and time window (10^{-7} s through 100 s). These measurements were carried out using the photon correlation spectroscopy (PCS) technique in right angle geometry, with laser wavelength = 647 nm and laser power = 200 mW. The vertically polarized incident beam was focused onto the sample mounted in an Oxford Optistat cryostat (temperature stability of ±0.1 K), and horizontally polarized scattered light was collected with a single mode optical fiber, split between two avalanche photodiode detectors, and cross-correlated using the ALV-7004/FAST multitau digital correlator.

Rheological creep compliance measurements were performed on the AR2000ex rheometer (TA Instruments) using 25 mm plates. The temperature of the sample was controlled in an environmental test chamber with liquid nitrogen as the gas source. At each measurement temperature, a constant small stress was applied until a steady state strain was achieved. The zero-shear viscosity was then extracted from the material response at the long time limit. In addition to creep measurements, dynamic mechanical measurements were carried out to obtain the mechanical spectrum in the frequency domain near T_g. Parallel plates of small diameter (4 mm) were used to minimize the contribution of instrument compliance.

RESULTS AND DISCUSSION

Figure 2 depicts the complex conductivity spectrum $\sigma^*(\omega)$ and the complex permittivity spectrum $\varepsilon^*(\omega)$ measured via BDS between 210 and 250 K. The frequency and temperature dependent dielectric spectra were analyzed with the Random Barrier Model proposed by Dyre[28−30] in order to extract the dc conductivity σ_0 and the characteristic ion diffusion rate $1/\tau_e$. These quantities were used to determine the temperature dependent ion diffusivity and free ion concentration in [m3oa][ntf2], as demonstrated below. In the Random Barrier Model, the complex conductivity spectrum can be analytically determined within the continuous time random walk approximation such that

$$\sigma^*(\omega) = \sigma_0\left(\frac{i\omega\tau_e}{\ln(1 + i\omega\tau_e)}\right) \quad (1)$$

It has been shown that eq 1 can describe well the conductivity spectrum of many aprotic room temperature ionic liquids.[31−33] Equation 1 also fits the conductivity spectrum of [m3oa][ntf2] well with only slight deviations near the crossover from ac to dc conduction and at high frequencies. The deviation in the lower frequency region is more clearly seen in the real permittivity spectrum (Figure 3). In order to account for this, an additional Cole−Cole relaxation function, found to have narrow dispersion ($\alpha_{CC} \approx 0.9$), was used to fit the spectra such that

dx.doi.org/10.1021/jp412365n | J. Phys. Chem. B 2014, 118, 783−790

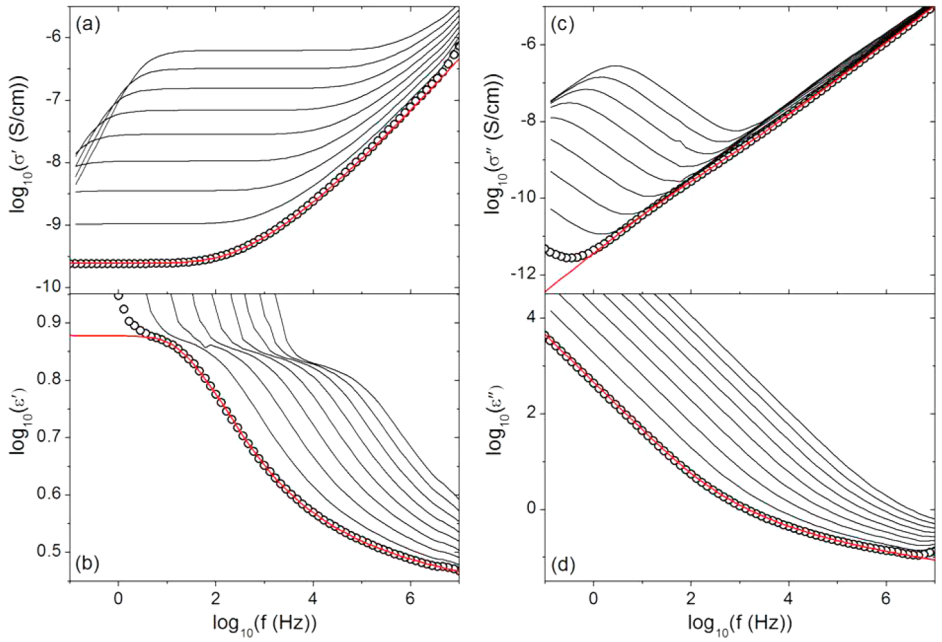

Figure 2. Real (a) and imaginary (c) parts of the complex conductivity spectrum $\sigma^*(\omega)$ as well as the real (b) and imaginary (d) parts of the complex permittivity spectrum $\varepsilon^*(\omega)$ are shown for selected temperatures (210–250 K in steps of 5 K). The data presented as open circles were measured at 210 K, and the red solid line is the fit to the spectrum using eq 2.

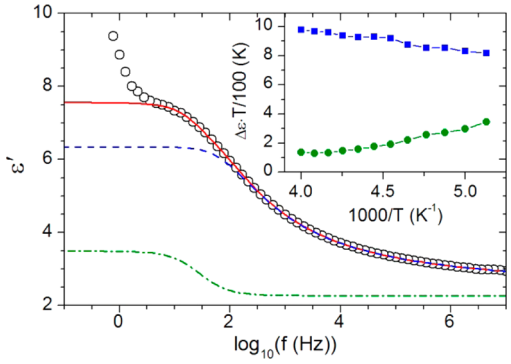

Figure 3. Real permittivity ε' measured at 210 K (open circles). The red solid line is the total fit of the data with eq 2, the blue dashed line is the contribution from the conductivity relaxation (random barrier model), and the green dash-dotted line is the contribution of the Cole–Cole function. The inset depicts the product $(\Delta\varepsilon \cdot T/100)$ for the conductivity relaxation process (blue squares) and the Cole–Cole relaxation process (green circles). Error bars are smaller than the symbols.

$$i\omega\varepsilon_0\varepsilon^*(\omega) = \sigma^*(\omega) = \sigma_0\left(\frac{i\omega\tau_e}{\ln(1 + i\omega\tau_e)}\right) + i\omega\varepsilon_0\left(\varepsilon_\infty + \frac{\Delta\varepsilon_{CC}}{1 + (i\omega\tau_{CC})^{\alpha_{CC}}}\right) \quad (2)$$

The relaxation times τ_e and τ_{CC} determined from the fits of the dielectric spectra are plotted against inverse temperature in Figure 7, and the temperature dependent dc conductivity is shown in Figure 4.

We have calculated the dielectric strength of the conductivity relaxation process according to the Random Barrier Model such that $\Delta\varepsilon = \sigma_0\tau_e/2\varepsilon_0$, where ε_0 is the vacuum permittivity, and compared it to the dielectric strength of the Cole–Cole process. As the temperature of the liquid is decreased, the

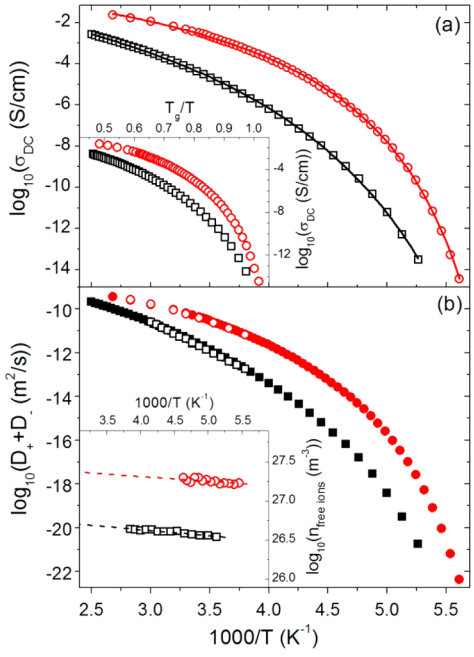

Figure 4. (a) dc conductivity plotted vs inverse temperature for [m3oa][ntf2] (black open squares) and for [bmim][ntf2] (red open circles). The corresponding lines are fits to the experimental data using the Vogel–Fulcher–Tammann equation. The inset depicts the same dc conductivity data plotted against T_g/T, where T_g = 186 K for [m3oa][ntf2] and T_g = 181 K for [bmim][ntf2]. (b) Total diffusivity $(D_+ + D_-)$ measured via PFG-NMR (open symbols) and BDS (solid symbols) for [m3oa][ntf2] (black squares) and [bmim][ntf2] (red circles). The inset depicts the total free ion concentration of [m3oa][ntf2] (open squares) and [bmim][ntf2] (open circles) calculated from eq 4 and the Arrhenius fits to these data (dashed lines).

product $(\Delta\varepsilon \cdot T)$ decreases slightly for the conductivity relaxation process, whereas it more than doubles for the

dx.doi.org/10.1021/jp412365n | J. Phys. Chem. B 2014, 118, 783–790

Cole−Cole relaxation process (see the inset of Figure 3). This decrease in the former case likely reflects the decreasing free ion concentration with decreasing temperature, while in the later case the increase may reflect the enhancement of dipolar correlations. Thus, it is possible that the small deviation accounted for by the Cole−Cole function may be a signature of a weak dipolar relaxation as suggested previously for the case of [bmim][ntf2].[33]

Since the molecular structure of [m3oa][ntf2] is comprised of a large fraction of nonpolar alkyl chains which are known to hydrophobically aggregate, it is probable that these inhomogeneities give rise to interfacial polarization effects. Thus it is also possible that this additional relaxation may be due to the Maxwell−Wagner−Sillers (MWS) effect.[34] We have estimated using the atomic van der Waals volumes that the charged regions of the molecule (cation and anion) account for approximately 35% percent of the total volume while the remaining alkyl chains comprise the remaining 65% percent. Assuming the alkyl chains have a temperature independent dielectric constant (ε_s = 2.3) and dc conductivity ($\sigma_{PE} = 10^{-17}$ S/cm)[35] identical to polyethylene and the ionic components are identical and spherical, we have calculated the relaxation time[34] of this interfacial polarization process as a function of temperature, such that

$$\tau_{MWS} = \varepsilon_0 \frac{(1-n)\varepsilon_{PE} + n\varepsilon_{ion} + n(\varepsilon_{PE} - \varepsilon_{ion})\varphi_{ion}}{(1-n)\sigma_{PE} + n\sigma_{ion} + n(\sigma_{PE} - \sigma_{ion})\varphi_{ion}} \quad (3)$$

where n = 0.33 for spherical particles, φ_{ion} is the volume fraction of the ionic component estimated above, ε_{PE} and ε_{ion} are the static dielectric constants of polyethylene and the measured conductivity relaxation process of the bulk liquid, respectively, and σ_{PE} and σ_{ion} are the conductivity of polyethylene and the measured dc conductivity of the bulk liquid, respectively. The MWS relaxation times calculated via eq 3 are plotted as a function of temperature in Figure 7. Surprisingly, the calculated MWS relaxation times agree quantitatively with the Cole−Cole relaxation times at all measurement temperatures. This quantitative agreement suggests that the deviation observed in Figure 3 may instead arise from interfacial polarization effects, and future studies will be performed to understand and characterize this feature in other types of ILs as well.

With the method proposed by some of the authors,[36] it is possible to quantitatively determine the temperature dependent free ion concentration and the ionic diffusivity using the characteristic ion hopping rate τ_e and the dc conductivity σ_0 extracted from the dielectric relaxation spectra. In their method, the electrodynamic analog of the Einstein relation, $\sigma_0 = (1/k_BT)(n_+D_+q_+^2 + n_-D_-q_-^2)$, is combined with the Einstein−Smoluchowski relation, $D = \lambda^2/2\tau_h$, to calculate the free ion concentration, where k_B is the Boltzmann constant, $n_{+,-}$ is the free ion concentration, $q_{+,-}$ is the ion charge, $D_{+,-}$ is the ion diffusivity, λ is the ion jump length, and $1/\tau_h \approx 1/\tau_e$ is the mean ion jump rate. Assuming that $D_+ \approx D_- = D$ (which has been demonstrated experimentally for many ILs[37]), $n_+ = n_- = n$, and $q_+ = q_- = e$ (the elementary charge), we arrive at the following expression connecting the free ion concentration, dc conductivity, and hopping rate, such that

$$\sigma_0 = \frac{2ne^2D}{k_BT} = \frac{ne^2\lambda^2}{k_BT\tau_e} \quad (4)$$

We have calculated the total free ion concentration ($n_{tot} = n_+ + n_-$) as a function of temperature in [m3oa][ntf2] via eq 4 using λ = 0.21 nm (λ is determined by matching the BDS diffusivity with the measured PFG NMR data and is assumed to be constant with temperature). It is seen in the inset of Figure 4b that the free ion concentration follows an Arrhenius type of thermal activation over this temperature range. We then calculated the ionic diffusivity of [m3oa][ntf2] over the entire temperature range using eq 4 and extrapolating the free ion concentration to high temperatures (assuming the same Arrhenius temperature dependence of free ions as found for low temperature). The diffusion coefficients determined via this BDS technique are shown in Figure 4b alongside the diffusion coefficients experimentally measured via PFG NMR. It is seen that the two methods to determine diffusion coefficients of [m3oa][ntf2] agree quantitatively, as has been demonstrated in studies of other ionic liquids.[25,31]

In order to understand how the dc conductivity, free ion concentration, and ion diffusion coefficients of [m3oa][ntf2] compare to those of other ionic liquids, we have plotted these data alongside the corresponding data of the ionic liquid [bmim][ntf2] in Figure 4. Measurements of [bmim][ntf2] were reported previously in ref 33. The hopping length λ reported in our previous study of [bmim][ntf2] was erroneously calculated because we had used an inaccurate form of eq 4 which did not account for contributions to dc conductivity from both positive and negative ions. We have reanalyzed the [bmim][ntf2] measurements in the identical manner as the presented measurements of [m3oa][ntf2] and have estimated the hopping length for this IL to be $\lambda \approx 0.11$ nm. The free ion concentration and diffusivity of [bmim][ntf2] presented in Figure 4b were calculated using this corrected hopping length.

Even though the glass transition temperatures of these two ILs are very similar (186 K compared to 181 K), it is immediately evident that the conductivity (shown in Figure 4a), free ion concentration, and ion diffusion coefficients of [m3oa][ntf2] are significantly lower than those of [bmim][ntf2]. At most temperatures, the dc conductivity and characteristic ion diffusion rates are at least 2 orders of magnitude lower for [m3oa][ntf2] while the free ion concentration is more than half an order of magnitude lower. It can be seen in Figure 4b that the diffusivities of the two ILs approach similar values at high temperature, which implies that the lower ion diffusion rate of [m3oa][ntf2] stems primarily from the more Arrhenius-like temperature dependence or lower dynamic fragility, m, where $m = \mathrm{d}\log_{10}(\tau)/\mathrm{d}(T_g/T)|_{T=T_g}$.[38] Nonetheless, Figure 4 explicitly demonstrates that the dramatic reduction of dc conductivity in this aprotic ammonium ionic liquid stems from both a reduced concentration of free ions as well as reduced ion mobility.

The reduction of free ion concentration may be the result of either a reduced number density of total ions in the system (i.e., density effects) or an enhancement of ion association in this liquid. To disentangle these two contributions, we have calculated the total percentage of free ions (% free ions = $n_{freeions}/n_{totalions}$) from measurements of the mass density at room temperature and from the calculated free ion concentration at 295 K. Using literature values of the density of [m3oa][ntf2] (ρ = 1.10 g/cm^3)[21] and [bmim][ntf2] (ρ = 1.44 g/cm^3)[37] at 295 K, we have determined that approximately 28% of the ions in [m3oa][ntf2] are free, while the percentage

dx.doi.org/10.1021/jp412365n | J. Phys. Chem. B 2014, 118, 783−790

of free ions is more than doubled for [bmim][ntf2], with approximately 57% of the ions free at room temperature. Clearly, the long chained [m3oa] cation exhibits an enhancement of ion association to the point where there is approximately only one-quarter of the ions in the system available for long-range conduction.

Having characterized the temperature dependent ionic conductivity, diffusivity, and free ion concentration, we now turn the focus to the measurements of structural dynamics via dynamic light scattering and rheology. Figure 5a depicts the

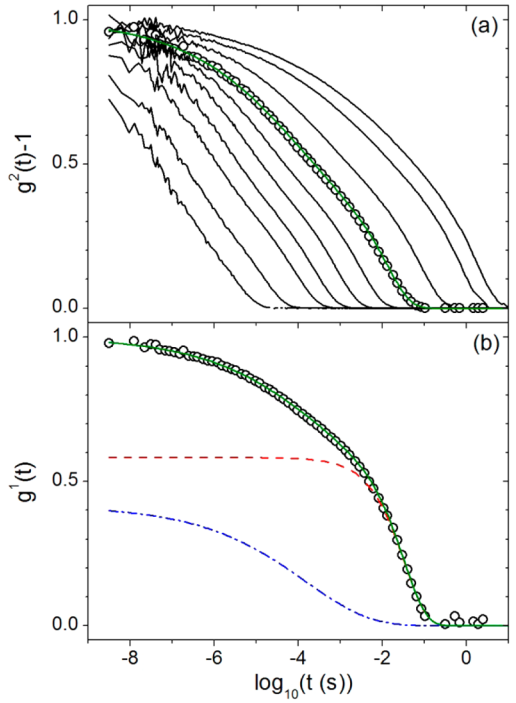

Figure 5. (a) Intensity correlation functions (ICF) measured by DDLS at 250, 240, 230, 225, 220, 215, 210, 205, 200, and 198 K from left to right. The ICF measured at 210 K is depicted with open circles, and these data have been fit using eq 5 (green solid line). (b) The field correlation function (FCF) measured at 210 K (open circles) is shown fit using eq 5. The FCF is clearly composed of two superimposed decays—one slower, Debye-like decay with $\beta_{slow} \approx 0.85$ (red dashed line) and one faster, highly stretched decay with $\beta_{fast} \approx 0.30$ (blue dash dotted line).

normalized intensity correlation functions (ICF) measured in [m3oa][ntf2] via DDLS. By visual inspection, it is immediately evident that the decay of the correlation function proceeds in two steps at all temperatures—one faster and highly stretched decay superimposed on top of a slower, narrower decay. We see no evidence for an additional, extremely slow relaxation process at any temperature such as that observed in recent rheological studies of [m3oa][ntf2].[26] The complex shape of the measured ICF is quite unique and has not been observed in DDLS measurements of other room temperature ionic liquids. In contrast, our recent studies of a series of imidazolium ionic liquids demonstrated that the ICF was found to decay with a single KWW stretched exponential function at all temperatures.[25] Additionally, a weak, faster secondary decay of the ICF was observed in these liquids at temperatures close to T_g which was assigned to the excess wing or Johari–Goldstein relaxation process found in the DDLS and BDS spectrum of molecular glass forming liquids.[39]

The ICFs measured in [m3oa][ntf2] were fit with a superposition of two KWW stretched exponential functions to extract the temperature dependent relaxation times and nonexponentiality (KWW) parameters of the two processes, such that

$$\mathrm{ICF} = g^2(t) - 1 = \gamma |g^1(t)|^2 = \gamma \left| a_1 \exp\left(-\left(\frac{t}{\tau_1}\right)^{\beta_1}\right) + a_2 \exp\left(-\left(\frac{t}{\tau_2}\right)^{\beta_2}\right)\right|^2 \quad (5)$$

where γ is the coherence factor of the optical system, a_1 and a_2 are the relative relaxation strengths, τ_1 and τ_2 are the characteristic relaxation times, and β_1 and β_2 are the nonexponentiality (KWW) parameters of the faster (1) and slower (2) decay processes, respectively.[40] Figure 5a depicts all measured, normalized ICFs with a fit of the experimental data using eq 5 at $T = 210$ K, while in Figure 5b, the same fit using eq 5 at 210 K is shown for the field correlation function, $g^1(t)$. The characteristic relaxation times τ_{KWW} were converted to the most probable relaxation times τ_{MAX} through the numerical Fourier transformation of the corresponding KWW function to the frequency domain, as described previously.[33] These relaxation times are plotted against inverse temperature in Figure 7. Both KWW parameters of the faster and slower relaxation processes were found to be roughly temperature independent at all measurement temperatures, with $\beta_{fast} \approx 0.3$ and $\beta_{slow} \approx 0.85$.

The light scattering spectrum of [m3oa][ntf2] is unique not only because it exhibits two relaxation processes but because it is also interesting that the dispersion of the slow relaxation process—which is approximately 2.15 orders of magnitude slower at all temperatures—is nearly Debye-like. Such evidence for a slow, mesoscopic relaxation process was reported by Turton et al. in Optical Kerr Effect (OKE) studies of a series of imidazolium based ILs with relatively short side chains.[6] In ref 6, the authors assigned the main peak of the measured spectrum to a pure Debye relaxation, and they assigned the structural α relaxation to the shoulder of this main peak. They found that these time scales were separated by less than 1 order of magnitude in all studied liquids. In contrast, Rivera et al. measured the light scattering spectrum of [bmim][PF6] using tandem Fabry–Perot interferometry in a similar frequency range and demonstrated that the peak feature could be described by a single Cole–Davidson (CD) function.[41] In our recent studies of a series of imidazolium ionic liquids, we also found a single peak in the DDLS spectrum for these liquids that could be fit well with a single CD function (or a KWW function), as mentioned above. While addressing the validity of these different fitting procedures is out of the scope of this paper, we do want to emphasize that the two step spectrum of [m3oa][ntf2] is unique, and the Debye-like feature found in this material may be of a different origin than the one observed by Turton et al.

Since there is such a clear evidence from DDLS measurements for a mesoscopic relaxation process in [m3oa][ntf2], it is reasonable to hypothesize that there may also be a signature of this Debye-like relaxation in the shear mechanical spectrum as well. In Figure 6, the frequency dependent real and imaginary shear moduli are shown at a reference temperature of 203 K, approximately 15 K above the calorimetric glass transition temperature. The mechanical spectrum exhibits the usual viscoelastic features of molecular liquids, and there is no

dx.doi.org/10.1021/jp412365n | J. Phys. Chem. B 2014, 118, 783–790

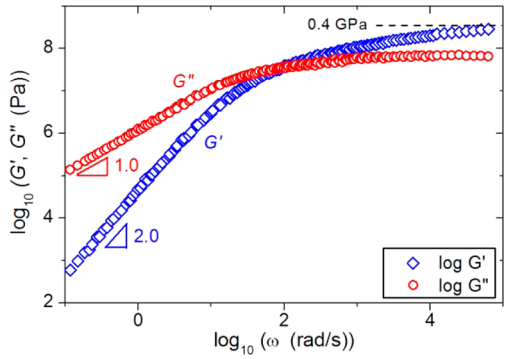

Figure 6. Superposed complex dynamic shear modulus is shown at reference temperature 203 K. The spectrum was constructed from measurements at several different temperatures using the time–temperature superposition principle.[47] The plateau shear modulus G_∞ was estimated to be approximately 0.4 GPa.

indication of a secondary, slow feature in the shear response of [m3oa][ntf2]. The plateau shear modulus G_∞ associated with the structural relaxation process was estimated to be approximately 0.4 GPa, as seen in Figure 6.

In order to better understand the physical origin of the two relaxations in the DDLS spectrum, we calculated the structural relaxation times from the measurements of zero-shear viscosity and the plateau shear modulus G_∞ using Maxwell's relation, $\tau_M = \eta/G_\infty$. It is expected that G_∞ varies only weakly over a broad temperature range in many glass forming liquids,[42] so we have calculated τ_M assuming $G_\infty = 0.4$ GPa for all temperatures. As is seen in Figure 7, τ_M calculated from rheological measurements

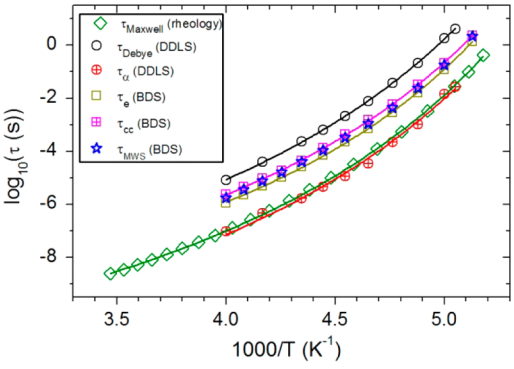

Figure 7. Characteristic time scales of charge transport and structural relaxation as measured via dielectric spectroscopy (BDS), dynamic light scattering (DDLS), and rheology are shown plotted against inverse temperature. The solid lines are fits to the data using the Vogel–Fulcher–Tammann equation. Error bars are smaller than the symbols.

is nearly identical to the fast relaxation times measured in DDLS. Thus, we assign the fast, nonexponential relaxation process to the structural α relaxation of [m3oa][ntf2]. To verify this assignment, we have also fit the fast relaxation times from DDLS with a Vogel–Fulcher–Tammann (VFT) function,[43,44] $\tau = \tau_0 \exp(A/(T - T_0))$, where τ_0, A, and T_0 are fit parameters, in order to calculate the dynamic glass transition temperature (at 100 s) and the dynamic fragility m. By extrapolating the VFT function to $\tau = 100$ s, we have determined the dynamic glass transition associated with the fast DDLS relaxation to be $T_g = 184$ K and the fragility $m \approx 60$. The dynamic glass transition temperature associated with τ_α (DDLS) agrees well with the calorimetric glass transition temperature ($T_g = 186 \pm 2$ K), which further verifies our assignment of the fast relaxation process to the structural α relaxation process in [m3oa][ntf2].

Having assigned the fast DDLS relaxation to the structural relaxation process, we now proceed to interpret the physical origin of the slow, Debye-like relaxation found in the DDLS spectrum. Clearly, this feature is related to motions of mesoscopic moieties because it is approximately 150 times slower than the structural relaxation process. Second, it is seen in Figure 7 that the slow relaxation process has a temperature dependence that is nearly identical to the temperature dependence of τ_α (DDLS), which implies that these two relaxations are closely related to one another.

Using the Debye–Stokes–Einstein (DSE) relation,[45,46] $\tau^{-1} = l(l + 1)k_BT/(8\pi\eta R^3)$, where $l = 2$ for light scattering rotational relaxation times and R is the hydrodynamic radius of the rotating unit, we have calculated the hydrodynamic diameter of this molecular moiety to be approximately $D_H \approx 1.2$ nm at all measurement temperatures. The hydrodynamic diameter estimated from the DSE relation agrees well with the static, supramolecular length scale ($d \approx 1.5$ nm) measured in recent small-angle X-ray scattering experiments on [m3oa][ntf2].[21] In this work and in a simulation study[22] of [m3oa][ntf2], such supramolecular length scales were determined to be connected to the presence of hydrophobic aggregates of the alkyl side chains. There is now significant evidence for the presence of hydrophobic aggregates in ammonium and phosphonium ionic liquids, and these aggregates become larger and more pronounced as the length of aliphatic side groups increases beyond approximately $n = 4$.[18−22] Since it is well established by structural and simulation studies that hydrophobic aggregates exist in the liquid state of [m3oa][ntf2], we tentatively assign the slow, Debye-like relaxation process observed in DDLS to the reorientational relaxation of relatively long-lived, aggregated alkyl nanodomains. We emphasize here that such mesoscopic scale relaxations have not been observed in other types of RTILs, such as [bmim][ntf2] and [bmim][pf6]. Further experiments on similar types of RTILs with long aliphatic side chains will be pursued in future work.

It is clearly seen in Figure 7 that the conductivity relaxation process has a significantly slower time scale than the structural α relaxation measured by rheology and DDLS, which implies that a hopping ion has an unusually slow transition rate between the free and associated state in [m3oa][ntf2]. It was demonstrated that, for imidazolium ILs, the conductivity relaxation rate is nearly identical or slightly faster than the structural relaxation rate, so that the rate of ion rotation is nearly identical to the rate of ion diffusion.[31] This unique property of [m3oa][ntf2] may arise due to the presence of larger concentrations of hydrophobic alkyl moieties in the liquid matrix. As larger concentrations of alkyl moieties are introduced to the IL, the cation and anion charge centers become spatially separated on longer length scales with larger and larger islands of hydrophobically aggregated nanodomains separating these charge centers. This picture of self-organization can be seen in the simulation studies of [m3oa][ntf2] and variations of this IL.[22] A consequence of this complex structural order is that as an ion center hops through the liquid matrix, a collective reorganization of the hydrophobic network must also occur, and furthermore, the diluting effect of the increasing length of the alkyl chain likely forces the ions to hop over longer distances. These two factors would cause the ion hopping process to occur less frequently,

dx.doi.org/10.1021/jp412365n | J. Phys. Chem. B 2014, 118, 783−790

which may explain why the ion diffusion rate is unusually slow in this IL and why the majority of ions are not free for long-range conduction. It is through this hypothetical physical picture that we suggest the unique ion conduction properties of [m3oa][ntf2] are strongly influenced by the presence of hydrophobic aggregates. Further experiments and simulations on other quaternary ammonium and phosphonium ILs, however, are required to corroborate this hypothesis.

CONCLUSION

Structural dynamics and charge transport in methyltrioctylammonium bis(trifluoromethylsulfonyl)imide [m3oa][ntf2] are characterized over a broad temperature range—from above the melting point down to the calorimetric glass transition temperature—using broadband dielectric spectroscopy, pulsed field gradient NMR, depolarized dynamic light scattering, and rheology. It is found that the magnitude of dc conductivity in [m3oa][ntf2] is substantially lower when compared to other ILs, such as [bmim][ntf2], and this reduction in dc conductivity can be traced back to both a lower number density of free ions in the liquid as well as a considerably slower ion diffusion process. In addition to the structural α relaxation, a slow Debye-like relaxation is observed in the DDLS spectra at all measurement temperatures. The Debye-like relaxation is more than 2 orders of magnitude slower than the structural α relaxation and is attributed to the reorientational motion of aggregated alkyl nanodomains. These findings indicate that the presence of hydrophobic aggregates significantly reduces ion mobility and also enhances counterion association in room temperature ionic liquids with extended aliphatic moieties.

AUTHOR INFORMATION

Corresponding Author

*E-mail: jsangoro@utk.edu.

Notes

The authors declare no competing financial interest.

ACKNOWLEDGMENTS

The authors gratefully acknowledge S. Naumov and J. Kärger (University of Leipzig) for help with PFG NMR measurements. The UT team thanks the NSF Chemistry program for funding (Grant CHE-1213444). Y.W. acknowledges funding through the LDRD program of Oak Ridge National Laboratory, managed by UT-Battelle, LLC, for the U.S. Department of Energy. J.R.S. thanks the University of Tennessee-Knoxville for financial support through tenure-track faculty research start-up funds. F.K. acknowledges the German Research Foundation (DFG) for financial support.

REFERENCES

(1) Sun, J.; MacFarlane, D.; Forsyth, M. Synthesis and Properties of Ambient Temperature Molten Salts Based on the Quaternary Ammonium Ion. *Ionics* **1997**, *3*, 356−362.

(2) Sun, J.; Forsyth, M.; MacFarlane, D. Room-temperature Molten Salts Based on the Quaternary Ammonium Ion. *J. Phys. Chem. B* **1998**, *102*, 8858−8864.

(3) McFarlane, D.; Sun, J.; Golding, J.; Meakin, P.; Forsyth, M. High Conductivity Molten Salts Based on the Imide Ion. *Electrochim. Acta* **2000**, *45*, 1271−1278.

(4) Urahata, S. M.; Ribeiro, M. C. Structure of Ionic Liquids of 1-alkyl-3-methylimidazolium Cations: A Systematic Computer Simulation Study. *J. Chem. Phys.* **2004**, *120*, 1855−1863.

(5) Canongia Lopes, J. N.; Pádua, A. A. Nanostructural Organization in Ionic Liquids. *J. Phys. Chem. B* **2006**, *110*, 3330−3335.

(6) Turton, D. A.; Hunger, J.; Stoppa, A.; Hefter, G.; Thoman, A.; Walther, M.; Buchner, R.; Wynne, K. Dynamics of Imidazolium Ionic Liquids From a Combined Dielectric Relaxation and Optical Kerr Effect Study: Evidence for Mesoscopic Aggregation. *J. Am. Chem. Soc.* **2009**, *131*, 11140−11146.

(7) Russina, O.; Triolo, A. New Experimental Evidence Supporting the Mesoscopic Segregation Model in Room Temperature Ionic Liquids. *Faraday Discuss.* **2012**, *154*, 97−109.

(8) Castner, E. W., Jr.; Wishart, J. F. Spotlight on Ionic Liquids. *J. Chem. Phys.* **2010**, *132*, 120901.

(9) Triolo, A.; Russina, O.; Fazio, B.; Triolo, R.; Di Cola, E. Morphology of 1-alkyl-3-methylimidazolium Hexafluorophosphate Room Temperature Ionic Liquids. *Chem. Phys. Lett.* **2008**, *457*, 362−365.

(10) Triolo, A.; Russina, O.; Bleif, H.-J.; Di Cola, E. Nanoscale Segregation in Room Temperature Ionic Liquids. *J. Phys. Chem. B* **2007**, *111*, 4641−4644.

(11) Triolo, A.; Russina, O.; Fazio, B.; Appetecchi, G. B.; Carewska, M.; Passerini, S. Nanoscale Organization in Piperidinium-based Room Temperature Ionic Liquids. *J. Chem. Phys.* **2009**, *130*, 164521.

(12) Beiner, M.; Huth, H. Nanophase Separation and Hindered Glass Transition in Side-chain Polymers. *Nat. Mater.* **2003**, *2*, 595−599.

(13) Hiller, S.; Pascui, O.; Budde, H.; Kabisch, O.; Reichert, D.; Beiner, M. Nanophase Separation in Side Chain Polymers: New Evidence from Structure and Dynamics. *New J. Phys.* **2004**, *6*, 10.

(14) Annapureddy, H. V.; Kashyap, H. K.; De Biase, P. M.; Margulis, C. J. What is the Origin of the Prepeak in the X-ray Scattering of Imidazolium-based Room-temperature Ionic Liquids? *J. Phys. Chem. B* **2010**, *114*, 16838−16846.

(15) Hettige, J. J.; Kashyap, H. K.; Annapureddy, H. V.; Margulis, C. J. Anions, the Reporters of Structure in Ionic Liquids. *J. Phys. Chem. Lett.* **2012**, *4*, 105−110.

(16) Kashyap, H. K.; Hettige, J. J.; Annapureddy, H. V.; Margulis, C. J. SAXS Anti-peaks Reveal the Length-scales of Dual Positive−negative and Polar−apolar Ordering in Room-temperature Ionic Liquids. *Chem. Commun.* **2012**, *48*, 5103−5105.

(17) Wang, Y.; Voth, G. A. Tail Aggregation and Domain Diffusion in Ionic Liquids. *J. Phys. Chem. B* **2006**, *110*, 18601−18608.

(18) Kashyap, H. K.; Santos, C. S.; Annapureddy, H. V.; Murthy, N. S.; Margulis, C. J.; Castner, E. W., Jr. Temperature-dependent Structure of Ionic Liquids: X-ray Scattering and Simulations. *Faraday Discuss.* **2012**, *154*, 133−143.

(19) Siqueira, L. J.; Ribeiro, M. C. Charge Ordering and Intermediate Range Order in Ammonium Ionic Liquids. *J. Chem. Phys.* **2011**, *135*, 204506.

(20) Santos, C. S.; Annapureddy, H. V.; Murthy, N. S.; Kashyap, H. K.; Castner, E. W.; Margulis, C. J. Temperature-dependent Structure of Methyltributylammonium Bis(trifluoromethylsulfonyl)amide: X-Ray Scattering and Simulations. *J. Chem. Phys.* **2011**, *134*, 064501.

(21) Pott, T.; Méléard, P. New Insight into the Nanostructure of Ionic Liquids: a Small Angle X-ray Scattering (SAXS) Study on Liquid Tri-alkyl-methyl-ammonium Bis(trifluoromethanesulfonyl)amides and Their Mixtures. *Phys. Chem. Chem. Phys.* **2009**, *11*, 5469−5475.

(22) Shimizu, K.; Pádua, A. l. A.; Canongia Lopes, J. N. Nanostructure of Trialkylmethylammonium Bistriflamide Ionic Liquids Studied by Molecular Dynamics. *J. Phys. Chem. B* **2010**, *114*, 15635−15641.

(23) Sangoro, J.; Iacob, C.; Serghei, A.; Naumov, S.; Galvosas, P.; Kärger, J.; Wespe, C.; Bordusa, F.; Stoppa, A.; Hunger, J. Electrical Conductivity and Translational Diffusion in the 1-butyl-3-methylimidazolium Tetrafluoroborate Ionic Liquid. *J. Chem. Phys.* **2008**, *128*, 214509.

(24) Krause, C.; Sangoro, J.; Iacob, C.; Kremer, F. Charge Transport and Dipolar Relaxations in Imidazolium-based Ionic Liquids. *J. Phys. Chem. B* **2009**, *114*, 382−386.

(25) Griffin, P. J.; Agapov, A. L.; Sokolov, A. P. Translation-rotation Decoupling and Nonexponentiality in Room Temperature Ionic Liquids. *Phys. Rev. E* **2012**, *86*, 021508.
(26) Mendil-Jakani, H.; Baroni, P.; Noirez, L.; Chancelier, L.; Gebel, G. Highlighting a Solid-Like Behavior in RTIL: Tri-Octyl-Methyl-Ammonium Bis(trifluoromethanesulfonyl)imide TOMA-TFSI. *J. Phys. Chem. Lett.* **2013**, *4*, 3775−3778.
(27) Stallmach, F.; Galvosas, P. Spin Echo NMR Diffusion Studies. *Ann. Rep. NMR Spectrosc.* **2007**, *61*, 51−131.
(28) Dyre, J. C. On the Mechanism of Glass Ionic Conductivity. *J. Non-Cryst. Solids* **1986**, *88*, 271−280.
(29) Dyre, J. C. The Random Free-energy Barrier Model for ac Conduction in Disordered Solids. *J. Appl. Phys.* **1988**, *64*, 2456−2468.
(30) Dyre, J. C.; Schrøder, T. B. Universality of ac Conduction in Disordered Solids. *Rev. Mod. Phys.* **2000**, *72*, 873−892.
(31) Sangoro, J. R.; Kremer, F. Charge Transport and Glassy Dynamics in Ionic Liquids. *Acc. Chem. Res.* **2011**, *45*, 525−532.
(32) Sangoro, J.; Iacob, C.; Naumov, S.; Valiullin, R.; Rexhausen, H.; Hunger, J.; Buchner, R.; Strehmel, V.; Kärger, J.; Kremer, F. Diffusion in Ionic Liquids: the Interplay Between Molecular Structure and Dynamics. *Soft Matter* **2011**, *7*, 1678−1681.
(33) Griffin, P.; Agapov, A. L.; Kisliuk, A.; Sun, X.-G.; Dai, S.; Novikov, V. N.; Sokolov, A. P. Decoupling Charge Transport from the Structural Dynamics in Room Temperature Ionic Liquids. *J. Chem. Phys.* **2011**, *135*, 114509.
(34) Kremer, F.; Schönhals, A. *Broadband Dielectric Spectroscopy*; Springer: Berlin, 2003.
(35) Adamec, V.; Calderwood, J. On the Determination of Electrical Conductivity in Polyethylene. *J. Phys. D: Appl. Phys.* **1981**, *14*, 1487−1494.
(36) Sangoro, J.; Serghei, A.; Naumov, S.; Galvosas, P.; Kärger, J.; Wespe, C.; Bordusa, F.; Kremer, F. Charge Transport and Mass Transport in Imidazolium-based Ionic Liquids. *Phys. Rev. E* **2008**, *77*, 051202.
(37) Tokuda, H.; Hayamizu, K.; Ishii, K.; Susan, M. A. B. H.; Watanabe, M. Physicochemical Properties and Structures of Room Temperature Ionic Liquids. 1. Variation of Anionic Species. *J. Phys. Chem. B* **2004**, *108*, 16593−16600.
(38) Böhmer, R.; Angell, C. A. Correlations of the Nonexponentiality and State Dependence of Mechanical Relaxations with Bond Connectivity in Ge-As-Se Supercooled Liquids. *Phys. Rev. B* **1992**, *45*, 10091−10094.
(39) Brodin, A.; Bergman, R.; Mattsson, J.; Rössler, E. Light Scattering and Dielectric Manifestations of Secondary Relaxations in Molecular Glassformers. *Eur. Phys. J. B* **2003**, *36*, 349−357.
(40) Berne, B. J.; Pecora, R. *Dynamic Light Scattering: With Applications to Chemistry, Biology, and Physics*; Wiley: New York, 1976.
(41) Rivera, A.; Brodin, A.; Pugachev, A.; Rössler, E. Orientational and Translational Dynamics in Room Temperature Ionic Liquids. *J. Chem. Phys.* **2007**, *126*, 114503.
(42) Dyre, J. C. Colloquium: The Glass Transition and Elastic Models of Glass-forming Liquids. *Rev. Mod. Phys.* **2006**, *78*, 953−972.
(43) Vogel, H. Das Temperaturabhängigkeitsgesetz der Viskosität von Flüssigkeiten. *Phys. Z* **1921**, *22*, 645−646.
(44) Fulcher, G. S. Analysis of Recent Measurements of the Viscosity of Glasses. *J. Am. Ceram. Soc.* **1925**, *8*, 339−355.
(45) Einstein, A. Zur Theorie der Brownschen Bewegung. *Ann. Phys.* **1906**, *324*, 371−381.
(46) Debye, P. J. W. *Polar Molecules*; Dover: New York, 1929.
(47) Ferry, J. D. *Viscoelastic Properties of Polymers*, 3rd ed.; Wiley: New York, 1980.